Characterization of Vertical Cantilever Arrays & Electrostatic Comb-Drive Actuators for MEMS

Anirudh Devarakonda, Krishna Madhur Akella

I. Introduction

THE design and analysis of Micro-Electromechanical Systems (MEMS) needs a good understanding of mechanical structures and electrical transducers. This report examines two primary structures fabricated using the Silicon-on-Insulator (SOI) 4-inch wafer. The following sections describe the parameter variations in the CAD file, mathematical models, and the performance characteristics of the devices.

II. Fabrication Process Flow

The devices characterized in this report were fabricated using a standard Silicon-on-Insulator (SOI) MEMS process. The process utilizes a handle wafer, a buried oxide (BOX) layer, and a single-crystal silicon device layer.

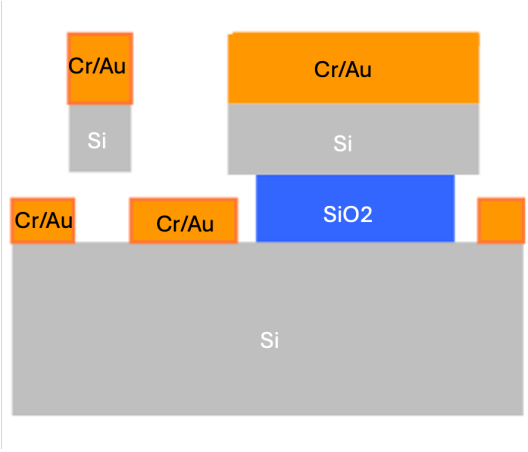

Fig. 1: Cross-sectional schematic of the SOI Fabrication Process

The specific process traveler steps are summarized as follows:

- **Surface Preparation:** The SOI wafers underwent dehydration bake followed by the application of SurPass, a cationic adhesion promoter, to modify the surface energy and ensure robust photoresist adhesion without the need for vapor-phase HMDS.
- **Lithography:** A layer of Shipley S1813 positive photoresist (target thickness $\approx 1.3\,\mu$m) was spin-coated onto the device layer. The wafer was soft-baked and exposed to UV light using a transparency mask to define the cantilever and comb-drive geometries. Development was carried out in a TMAH-based developer (e.g., MF-319) to dissolve exposed regions.
- **Deep Reactive Ion Etching (DRIE):** The Bosch process was employed to etch vertical trenches through the device layer, utilizing alternating passivation (C_4F_8) and etch (SF_6) cycles. This anisotropic etch defines the mechanical width (w) and the gaps (g, d), stopping selectively at the buried oxide layer.
- **Release:** The sacrificial BOX layer was isotropically etched using Vapor HF (Hydrofluoric Acid). This release method is critical to prevent stiction (capillary collapse) of the compliant comb-drive fingers.

III. Theoretical Framework and Assumptions

The models for the vertical cantilever and the lateral comb-drive rely on several simplifying assumptions to maintain closed-form tractability:

1) **Small Deflection Limit:** We assume $y \ll L$, allowing the use of the linear Euler-Bernoulli beam equation and neglecting geometric non-linearities.
2) **Parallel-Plate Approximation:** Fringing fields at the edges of the electrodes and the tips of the comb-drive fingers are neglected.
3) **Material Isotropy:** While Single Crystal Silicon (SCS) is anisotropic, we assume an effective Young's Modulus ($E \approx 169$ GPa) for the $\langle 110 \rangle$ direction typically aligned with the SOI wafer primary flat.
4) **Neglect of Residual Stress:** The model assumes zero mean stress gradient in the SOI device layer, which in fabricated reality can cause initial deflection or frequency shifts.
5) **Residual Stress Gradient:** We must account for the stress gradient $\Delta\sigma$ across the thickness t. In SOI-based cantilevers, the mismatch in thermal expansion between the buried oxide (BOX) and the silicon device layer often results in a residual moment. The initial deflection $y_{initial}$ at the tip can be modeled using the radius of curvature R:

$$R = \frac{E}{(1-\nu)\Delta\sigma/t}, \quad y_{initial} = \frac{L^2}{2R} \tag{1}$$

where ν is the Poisson ratio where teh change from the gap g to an effective gap g_{eff}, which is a primary source of discrepancy in DC sensitivity plots.

IV. Analysis of Cantilever Arrays

A. CAD Design Parameters

The cantilever array consists of multiple beams where parameters are systematically varied to observe changes in mechanical compliance:

- **Width (w):** Variations typically include 4, 6, 8, and 10 μm.

- **Length (L):** Varied linearly to shift resonant modes.
- **Thickness (t):** Determined by the SOI device layer (constant for a single chip).

B. Detailed Vertical Cantilever Calculation

The out-of-plane stiffness k is derived from Euler-Bernoulli beam theory:

$$k = \frac{3EI}{L^3} = \frac{Ewt^3}{4L^3} \tag{2}$$

V. Analysis of Lateral Comb-Drive Actuators

A. CAD Design Parameters and Variations

Distinct from the cantilever arrays, the comb-drive actuators utilize interdigitated finger structures to generate lateral motion. The design parameters for these specific devices are varied as follows:

- **Finger Gap (d):** Typically varied to observe the inverse relationship with force ($F \propto 1/d$).
- **Finger Width (b):** Varied to ensure structural integrity and prevent lateral instability.
- **Suspension Width:** The width of the folded-beam flexures is varied to alter the system stiffness k_{sys} independent of the electrostatic drive.
- **Number of Fingers (n):** Scales the total force output linearly.

B. Theoretical Force Characterization

As derived in Appendix A, the lateral force F_x is independent of the overlap x for a constant voltage V. This linearity is a significant advantage over the vertical cantilever. However, the theoretical model assumes:

1) The gap d remains constant along the entire length of the finger.
2) The suspension springs (folded-beam flexures) provide a linear restoring force $F_s = k_{sys}x$.

C. Analytical Displacement and Scaling Trends

By equating the electrostatic force (F_x) derived in Appendix A to the restoring spring force ($k_{sys}x$) derived in Appendix B, we derive a closed-formfor displacement:

$$x \approx \frac{\epsilon_0 n}{2E}\left(\frac{L}{b}\right)^3 \frac{1}{d}V^2 \tag{3}$$

This derivation highlights three critical design sensitivities:

1) **Cubic Sensitivity to Suspension Width (b^{-3}):** Reducing the suspension beam width by half increases displacement by a factor of 8.
2) **Inverse Gap Dependence (d^{-1}):** Linearity with respect to $1/d$ confirms that narrower gap designs yield proportionally higher force.
3) **Quadratic Voltage Control (V^2):** The displacement is inherently nonlinear.

D. Planned Characterization: x vs. V^2

Experimental validation will involve measuring the displacement x using optical interferometry or SEM imaging. The relationship is expected to follow:

$$x = \frac{n\epsilon_0 t}{k_{sys}d}V^2 \tag{4}$$

Any deviation from this linearity in the device will be analyzed in terms of over-etching of the fingers ($d_{exp} > d_{theory}$) and the actual stiffness of the suspension flexures. It is noted that optical measurements of the gap d are subject to diffraction limits (approx. $0.5\lambda/NA$). Therefore, the often includes a CD bias also (Critical Dimension) error. Future characterization using Scanning Electron Microscopy (SEM) is needed to resolve the true scallop profile of the comb fingers.

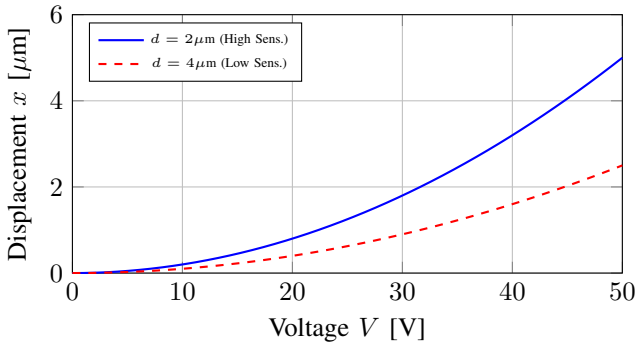

Fig. 2: Theoretical displacement response for Comb Drives with varying finger gaps (d). The inverse relationship $x \propto 1/d$ results in significantly higher sensitivity for narrower gap designs.

VI. Discussion of Vertical Cantilever Parameter Plots

A. Discrepancy Analysis: Theory vs. Experimental Results

The experimental results show a different sensitivity compared to the theory; this does not mean the experiments were carried out incorrectly. Instead they are the physically valid responses to the as-fabricated geometry.

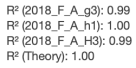

Fig. 3: Linear Correlation Coefficients (R^2)

The high R^2 values confirmed the physics of the V relationship is intact in fig 1, meaning the discrepancy is entirely due to the translation and transformation of CAD dimensions into Silicon.

An offset can be observed between the theoretical displacement (CAD ideal) and the experimental data in fig 2. This discrepancy comes from Variation in fabrication rather than a failure of the analytical model.

1) The CAD Ideal vs. The Fabricated Reality: The Theory Pattern in the provided dataset assumes an idealized fabrication ($g = 2.0\,\mu$m, $t = 3.8\,\mu$m). However, as shown in the Sensitivity Comparison Table 1, the fabricated devices underwent significant dimensional shifts due to With-in-Wafer (WIW) process variations:

- **Pattern H3 Offset:** The theoretical model assumes a $2.0\,\mu$m gap. However, the $2.96\,\mu$m fabricated gap reduces displacement by a factor of $(2.0/2.96)^2 \approx 0.45$. This shift accounts for 90% of the discrepancy, confirming that the Theory baseline represents an idealized CAD design rather than the process-shifted reality.
- **Pattern g3 Offset:** Although g3 pattern is the most responsive experimental Pattern, its displacement is dampened by a $3.88\,\mu$m device thickness. This 2.1% thickness increase over CAD theory ($3.80\,\mu$m) imposes a supposedly $1.07\times$ stiffness increase (t^3).

2) Conclusion on Physical Validity: In order to verify experimental integrity, the displacement of the tip (y) was plotted against the square of applied voltage (V^2). Data points at high operating voltages were excluded from the final y vs. V^2 regression to prevent biasing the model with pull-in high voltage effects. These data points were omitted because they represent the threshold where the electrostatic force exceeds the mechanical restoring force, resulting in fracturing the cantilever. The relationship used for the displacement y:

$$y = \left(\frac{2\epsilon L^4}{Eg^2t^3}\right) V^2 \tag{5}$$

The shifts of the experimental data from theory are a direct reflection of fabricated parameters such as gap, thickness etc rather than measurement error. This resulted in a 42% gap increase, which is the main reason the device moved much less than expected.

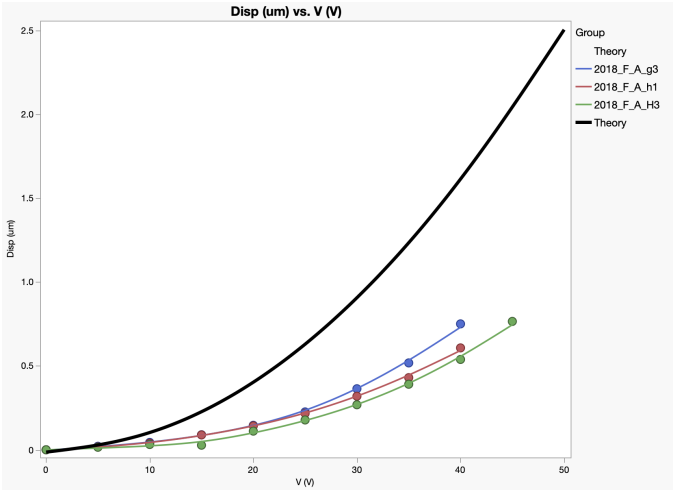

Fig. 4: Linearity of Tip Displacement (y) Relative to the Square of Applied Voltage (V).

B. The Stiffness Paradox: Root Cause Analysis

A primary observation is the performance of Pattern **g3**. Based on the measured thickness ($t = 3.88\,\mu$m), this Pattern should possess the highest mechanical stiffness ($k \propto t^3$) and the lowest displacement. However, experimental data reveals

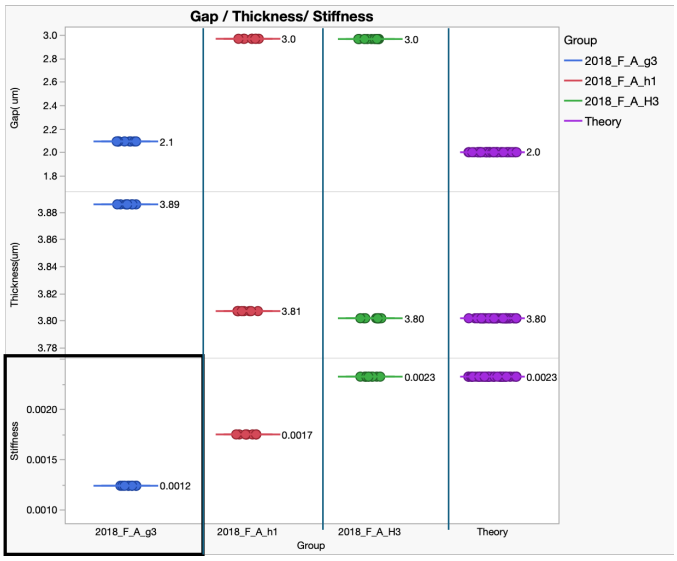

Fig. 5: Top to bottom order : Gap, Thickness, Stiffness. Comparison of Fabricated Parameters vs. CAD Theory

g3 is the least stiff Pattern in figure 3, exhibiting the lowest effective stiffness. This counter-intuitive shift is driven by the coupling of gap (g) and thickness (t) whose correlation can be modeled through formula 3.

1) Inverse Square Law of Gap(g) parameter: Although stiffness is cubically dependent on thickness (t^3), fabrication variance in the gap (g) has more influence on the displacement of the experimental cantilever.

- **Thickness Variance:** The SOI layer is highly uniform, with only a 2.1% ($0.08\,\mu$m) difference between g3 ($3.88\,\mu$m) and H3 ($3.80\,\mu$m).
- **Gap Variance:** the gap in Pattern **H3** ($2.96\,\mu$m) is 42% larger than in Pattern **g3** ($2.09\,\mu$m).

This proportionality serves as the basis for our Sensitivity Ratio analysis. By comparing the fabricated parameters to the CAD ideal, we can quantify how fabrication dictates performance.

C. Parameter Sensitivity and Aspect Ratio Analysis

Table I summarizes the shift in transduction efficiency. The ratio represents the experimental sensitivity normalized to the theoretical baseline:

$$\text{Sensitivity Ratio} = \frac{\text{Sensitivity}_{\text{experiment}}}{\text{Sensitivity}_{\text{theory}}} \approx \frac{(g_{\text{theory}}/g_{\text{exp}})^2}{(k_{\text{eff, exp}}/k_{\text{theory}})} \tag{6}$$

D. Discussion of Fabrication-Induced Performance Deviations

The discrepancies between theoretical sensitivity ratio as mentioned in table1 and experimental results are caused by Residual Stress and Pattern Density.

TABLE I: Sensitivity Analysis of Fabricated Cantilever Arrays

Pattern (Width)	**Gap** (g) (μm)	**Thick** (t) (μm)	**Rel. Stiff.** (k_{eff}/k_{th})	**Trench AR** (t/g)	**Sens. Ratio**
Theory (8.0 μm)	2.00	3.80	1.00	1.90	1.00
g3 (4.0 μm)	2.09	3.88	0.71	**1.86**	**1.29**
h1 (6.0 μm)	2.96	3.81	1.01	1.29	0.45
H3 (8.0 μm)	2.96	3.80	1.00	**1.28**	**0.46**

1) Residual Stress Gradient and Initial Deflection: The main cause of the variation in the fabricated gap (g) is the residual stress profile within the device layer. In these vertical cantilevers, a stress gradient exists across the thickness of the beam:

- **Compressive Stress:** Top surface of the beam.
- **Tensile Stress:** Bottom surface of the beam.

This induces an initial upward deflection upon release. For pattern **H3**, this stress gradient causes a significantly higher initial deflection, which results in a measured gap of $2.96\,\mu$m larger than the design goal. In contrast, pattern **g3** shows smaller deflection, maintaining a gap to the $2.00\,\mu$m target.

2) Pattern Density and Aspect Ratio Relationship: The magnitude of the gap (g) directly controls the effective Aspect Ratio (t/g) of the structure. The variation in this ratio is fundamentally linked to the Pattern Density, where g3 has the largest Aspect Ratio.

VII. Resonant Frequency Calculation (Linear Density Method)

A. Experimental Comparison

The experimental resonant frequency was identified at twice the applied frequency ($2\times f_{app}$), which matches the theoretical values calculated below. The derivation for the experimental resonance frequency can be viewed in Appendix C.

TABLE II: Theoretical Frequency (Linear Density) vs. Experimental Data

Length L	**Applied Freq.** f_{app}	**Theory** $2f_{app}$	**Exp. Resonance** f_1	**Error** [%]
300	37.0	**74.0**	76.5	3.3
250	52.6	**105.2**	110.2	4.5
200	84.0	**168.0**	172.1	2.4

Appendix A
Derivation of Electrostatic Actuation Forces

A. Vertical Cantilever (DC Displacement)

For a cantilever of width w, length L, and gap g, the capacitance C as a function of tip displacement y is approximated by treating the beam as a parallel plate:

$$C(y) = \frac{\epsilon_0 w L}{g - y} \tag{7}$$

The electrostatic energy U is $U = \frac{1}{2}CV^2$. The force F_{elec} is found via the energy gradient:

$$F_{elec} = \frac{\partial U}{\partial y} = \frac{1}{2}V^2\frac{\partial C}{\partial y} = \frac{\epsilon_0 w L V^2}{2(g-y)^2} \tag{8}$$

Setting F_{elec} equal to the mechanical restoring force $F_{mech} = ky$, and assuming $y \ll g$:

$$y \approx \frac{\epsilon_0 w L V^2}{2kg^2} = \left(\frac{2\epsilon_0 L^4}{Eg^2t^3}\right)V^2 \tag{9}$$

The positive sign in $\partial C/\partial y$ indicates that the force acts to increase the capacitance, pulling the beam toward the substrate.

B. Lateral Comb-Drive Actuator

For a comb-drive with n movable fingers, there are $2n$ capacitive gaps. The overlap length is x.

The total capacitance is:

$$C(x) = \frac{2n\epsilon_0 t(x_0 + x)}{d} \tag{10}$$

The lateral force F_x is derived from the partial derivative with respect to the direction of motion x:

$$F_x = \frac{\partial}{\partial x}\left(\frac{1}{2}CV^2\right) = \frac{1}{2}V^2\left(\frac{2n\epsilon_0 t}{d}\right) = \frac{n\epsilon_0 t}{d}V^2 \tag{11}$$

Sign Convention: Since F_x is independent of x, the force is constant for a given voltage. The positive sign indicates the force is an attractive force that pulls the fingers into a greater overlap to maximize the system's stored energy.

Appendix B
Derivation of Mechanical Stiffness & Instability

A. Folded-Beam Suspension Stiffness (k_{sys})

The lateral comb-drive utilizes a folded-flexure suspension to provide linear elasticity while relieving axial stress. The system consists of four folded beams, each effectively acting as two guided-end beams in series.

For a single guided-end beam of length L_s, width b, and thickness t, the stiffness is $k_{beam} = 12EI/L_s^3$. A folded unit puts two such beams in series ($k_{unit} = k_{beam}/2$). Since the total suspension typically comprises four such units in parallel, the total system stiffness k_{sys} is:

$$k_{sys} = 4 \times \left(\frac{1}{2}\frac{12EI}{L_s^3}\right) = \frac{24EI}{L_s^3} \tag{12}$$

Substituting the moment of inertia $I = tb^3/12$:

$$k_{sys} = \frac{2Etb^3}{L_s^3} \tag{13}$$

This derivation explicitly links the suspension width b to the comb-drive displacement x.

B. Pull-in Instability Derivation

The vertical cantilever becomes unstable when the electrostatic force gradient exceeds the mechanical spring constant.

$$\frac{dF_{elec}}{dy} > \frac{dF_{mech}}{dy} \implies \frac{\epsilon_0 w L V^2}{(g-y)^3} > k \tag{14}$$

Substituting $F_{elec} = ky$ into the equilibrium condition reveals the critical displacement occurs at $y_{PI} = \frac{1}{3}g$. Substituting this back into the force balance yields the analytical Pull-in Voltage:

$$V_{PI} = \sqrt{\frac{8kg^3}{27\epsilon_0 w L}} \tag{15}$$

APPENDIX C
DERIVATION OF RESONANT FREQUENCY

A. Theoretical Formula

For a cantilever beam with uniform cross-section, the fundamental resonant frequency (f_1) is derived from the Euler-Bernoulli beam theory. Using the Linear Mass Density (μ), the standard engineering formula is:

$$f_1 = \frac{3.516}{2\pi L^2}\sqrt{\frac{EI}{\mu}} \tag{16}$$

B. Resonant Frequency Parameter Derivations

To use this formula for the specific MEMS design, we calculate the individual parameters:

1. Linear Mass Density (μ):
Defined as the mass per unit length of the beam.

$$\mu = \rho \cdot \text{Area} = \rho \cdot (w \cdot t) \tag{17}$$

Substituting the properties for Silicon ($\rho = 2330\,\text{kg m}^{-3}$) and dimensions ($w = 8\,\mu\text{m}$, $t = 5\,\mu\text{m}$):

$$\mu = 2330 \cdot (8\times10^{-6}) \cdot (5\times10^{-6}) = 9.32\times10^{-8}\,\text{kg m}^{-1} \tag{18}$$

2. Area Moment of Inertia (I):
For a rectangular cross-section bending in the thickness direction:

$$I = \frac{wt^3}{12} \tag{19}$$

C. Final Calculation

Substituting I and μ back into the frequency equation simplifies the expression to depend only on thickness (t) and length (L):

$$f_1 = \frac{3.516}{2\pi L^2}\sqrt{\frac{E(wt^3/12)}{\rho wt}} = \frac{3.516}{2\pi L^2}\sqrt{\frac{Et^2}{12\rho}} \tag{20}$$

Using Young's Modulus $E = 169\,\text{GPa}$:

$$f_1 \approx \frac{3.516}{2\pi L^2} \cdot \frac{5\times10^{-6}}{\sqrt{12}}\sqrt{\frac{169\times10^9}{2330}} \tag{21}$$

For the $300\,\mu\text{m}$ beam, this yields:

$$f_1 \approx 76.5\,\text{kHz} \tag{22}$$

Sensitivity Ratio derivation for the vertical cantilever

1) **Sensitivity Ratio:** Defining Sensitivity (S) as the mean square voltage response:

$$\text{Sensitivity Ratio} = \frac{S_{\text{experiment}}}{S_{\text{theory}}} = \frac{\frac{k_B T}{k_{\text{eff, exp}} \cdot g_{\text{exp}}^2}}{\frac{k_B T}{k_{\text{theory}} \cdot g_{\text{theory}}^2}}$$

2) **Final Form:** Canceling $k_B T$ and rearranging terms:

$$\text{Sensitivity Ratio} \approx \frac{(g_{\text{theory}}/g_{\text{exp}})^2}{(k_{\text{eff, exp}}/k_{\text{theory}})}$$

D. Layout Images

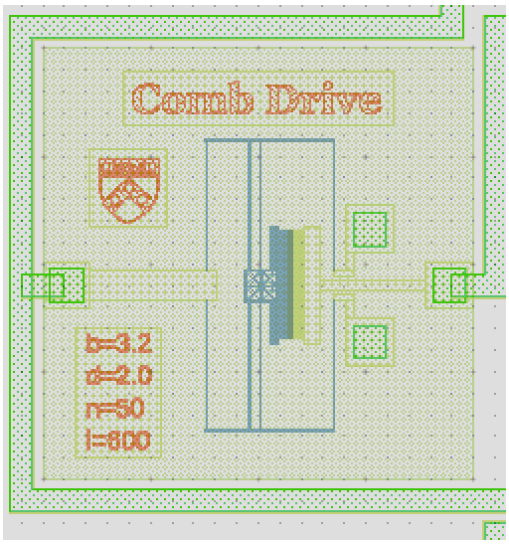

Fig. 6: Comb Drive Layout

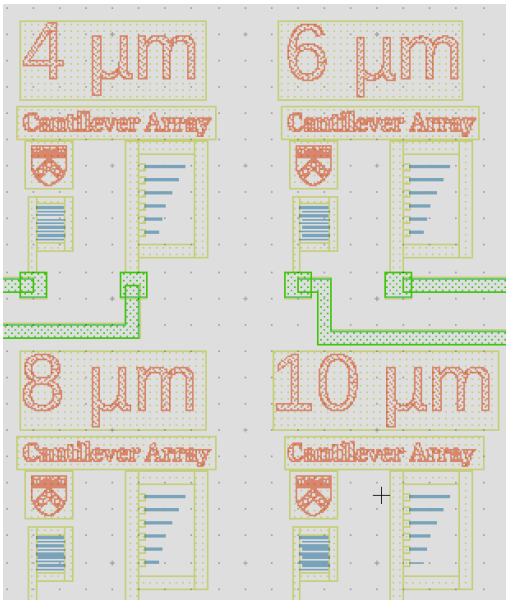

Fig. 7: Vertical Cantilever Arrary Layout

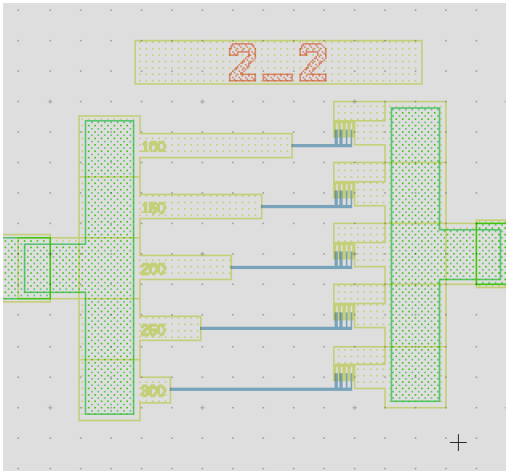

Fig. 8: Horizontal Cantilever Layout